Research Article | Vol. 61, No. 33 / 20 November 2022 / Applied Optics 10021

applied optics

Analysis and design of a wide-field and large-numerical-aperture compact imaging spectrometer with a freeform surface

Jialun Zhang,[1,2] Yuquan Zheng,[1,2,*] Chao Lin,[1,2] Zhenhua Ji,[1,2] Yanxue Han,[1,2,3] and Yi Shi[1,2,3]

[1]Changchun Institute of Optics, Fine Mechanics and Physics, Chinese Academy of Sciences, Changchun 130033, China
[2]State Key Laboratory of Applied Optics, Changchun Institute of Optics, Fine Mechanics and Physics, Chinese Academy of Sciences, Changchun 130033, China
[3]University of Chinese Academy of Sciences, Beijing 100049, China
*Corresponding author: zhengyq@sklao.ac.cn

Received 10 August 2022; revised 25 September 2022; accepted 26 September 2022; posted 29 September 2022; published 17 November 2022

Wide-field-of-view (FoV) Offner imaging spectrometers with freeform surfaces have been studied extensively in recent years. However, a design result with a large numerical aperture (NA) cannot be simultaneously obtained with this layout. We present the concept of a limited system in the tangential direction. Based on this insight, we present a new design method, to the best of our knowledge, based on the decenter anamorphic stop, which can achieve large NA in compact wide-FoV Offner imaging spectrometers with freeform surfaces. Compared to conventional imaging spectrometers with the same parameters, the light-gathering capacity of the decenter anamorphic stop-based imaging spectrometer is increased by more than 40%. In addition, based on the presented method, we design a compact imaging spectrometer with a wide FoV and large NA. The designed imaging spectrometer with a freeform surface has excellent performance. Finally, we fabricate and measure the freeform mirror. The surface irregularity of the freeform mirror is better than $1/30\lambda$ ($\lambda = 632.8$ nm). The result shows that the Offner imaging spectrometer with a freeform surface can be fabricated and will play a significant role in the fields of aeronautical and astronautical remote sensing.

https://doi.org/10.1364/AO.472164

1. INTRODUCTION

Compared with traditional spherical and aspheric surfaces, freeform surfaces offer more degrees of design freedom for optical design [1]. Therefore, freeform surfaces have received considerable attention in the last decade, and there have been significant advances in testing and manufacturing technology [2]. Initially, freeform surfaces were applied to non-imaging systems, such as LED lighting systems [3,4]. Today, freeform surfaces have made their mark in various imaging applications such as off-axis reflective telescope systems, helmet displays, and zoom systems [5,6].

Hyperspectral imaging technology, which was proposed in the 1980s, combines spectral analysis with remote sensing imaging. After more than 30 years of development, it has become an important part of aerospace remote sensing. However, the development of new unmanned aerial vehicle (UAV) technologies has led to additional requirements for airborne imaging spectrometers. For example, higher efficiency, higher spectral and spatial resolution, wider working spectra, and more compact sizes are desired in agricultural remote sensing. Many of these requirements are mutually incompatible from the perspective of optical design and cannot be easily addressed by traditional solutions.

Freeform optics provides an important approach for solving the above problems. In recent years, the study of imaging spectrometers with freeform surfaces has become an important part of freeform optics. In 2016, Peschel *et al*. designed a freeform mirror that can be described by Zernike polynomials. The Offner imaging spectrometer includes only a freeform mirror and a convex grating, which reduces the difficulty of imaging spectrometer alignment [7]. In 2017, Reimers *et al*. presented designs for two freeform imaging spectrometers based on Offner–Chrisp geometry. One design is based on a freeform grating and the other on a hybrid spherical-freeform Mangin grating. The imaging spectrometers have significantly increased spectral bandwidth and slit length [8]. In 2018, Yang *et al*. proposed a point-by-point approach for designing freeform imaging spectrometers [9]. In 2019, Feng *et al*. designed a freeform imaging spectrometer that uses curved prisms as dispersive elements to achieve ultra-wideband detection [10]. In 2019, Shafer *et al*. compared Offner imaging spectrometers designed by spherical, aspherical, and freeform surfaces, respectively. The field can be significantly widened by using freeform surfaces [11]. In 2021, Zhang *et al*. proposed an analysis method for Offner imaging spectrometers based on vector aberration theory (VAT). VAT provides strong support for the design of wide-field-of-view (FoV) compact imaging spectrometers with the freeform surface [12]. In general, Offner imaging spectrometers have advantages for achieving designs with wide FoVs [13,14]. However, the NA of an Offner imaging spectrometer is limited by its symmetrical structure. We refer to an optical system with such a limit as a limited system in the tangential direction in this paper. The size of the NA is the most critical factor for compact imaging spectrometer designs. Increasing the NA of an imaging spectrometer is extremely important for improving its detection capability. However, even with the application of freeform optics, wide FoV, large NA, and compactness still cannot be simultaneously achieved with the above designs.

To address this problem, we propose a decenter anamorphic stop for Offner imaging spectrometers. In a limited system in the tangential direction in which the tangential NA cannot be increased, unilaterally increasing the sagittal NA offers a compromise solution. The method plays a significant role in the design of a compact wide-FoV and large-NA imaging spectrometer with freeform optics.

The remainder of this paper is organized as follows. In Section 2, we consider the Offner imaging spectrometer to be a special type of limited system in the tangential direction and present a decenter anamorphic stop-based design approach for a compact Offner imaging spectrometer with a wide FoV and large NA utilizing a freeform surface. In Section 3, we provide the design results for an imaging spectrometer with a freeform surface. The performance of the design results is also discussed and analyzed. In Section 4, we fabricate and measure the freeform mirror. The process of the fabrication and the result of the metrology are introduced, respectively. Finally, we conclude the paper and present our future research plans.

2. DESIGN METHOD FOR A WIDE-FOV AND LARGE-NA COMPACT OFFNER IMAGING SPECTROMETER

A. Limited System in the Tangential Direction

Ray obstruction is one of the most important problems in the realization of compact designs for Offner imaging spectrometers [12]. VAT analysis of the Offner imaging spectrometer indicates that, to achieve a design without obstructions, the equivalent field decenter vector of the system should be increased. This, however, causes a large increase in the aberration. Therefore, achieving a reasonable balance between the NA and the size of the imaging spectrometer becomes an empirical problem. The dispersion direction of the conventional Offner imaging spectrometer is entirely tangential. As shown in Fig. 1, the fact that the dispersion direction of the imaging spectrometer is along the same direction as the folding direction imposes a serious spatial constraint on the structure of the imaging spectrometer. We refer to a system subjected to such constraints as a limited system in the tangential direction.

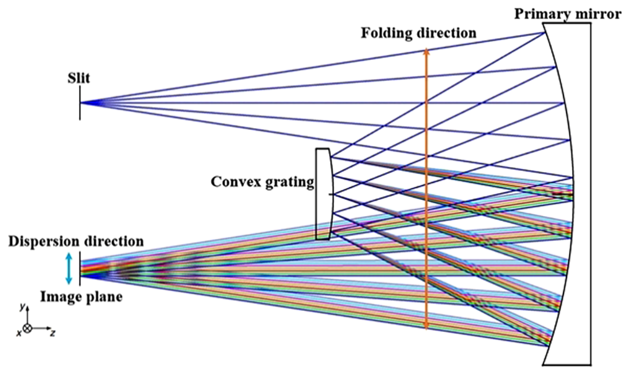

Fig. 1. Schematic diagram of a limited system in the tangential direction of the Offner grating imaging spectrometer.

In some designs, the f-number of the Offner imaging spectrometer is reduced to 2.2. The f-number is usually reduced by cutting a part of the convex grating or through the use of advanced aberration correction grating designs [15]. However, these methods cannot simultaneously achieve a wide FoV. Fuerschbach *et al*. used nodal aberration theory to show that the aberration contribution of the aperture stop is a constant for a given field and that an aberration correction grating with a complex surface or a varied-line spacing grating cannot compensate for field aberration [16]. However, increasing the number of freeform optical components in the system significantly increases the difficulties in testing and manufacturing the system. Therefore, designing a compact imaging spectrometer with a wide FoV and large NA becomes a challenge when only one free optical element can be used in the system.

B. Design Method of the Decenter Anamorphic Stop

The Offner imaging spectrometer is a telecentric optical system, and it is not intuitive to discuss numerical aperture directly [17]. Based on geometrical optics, if the focal length of the optical system is fixed, then the NA can be characterized by the entrance pupil diameter. Hence, we consider using some intuitive parameters to represent the NA in the Offner imaging spectrometer.

The three optical elements that are concentric and satisfy the Rowland circle condition are the main structural features of the Offner imaging spectrometer [13,14]. In Fig. 2(a), the relationship between the position and curvature of the primary and secondary mirrors of the Offner imaging spectrometer is clear. And Fig. 2(b) is an on-axis Offner structure, which has the characteristic of the object and image point having the same position. At paraxial conditions, parameters of the optical element, such as the mechanical diameter, can be calculated more easily. Further, we can obtain the size of the secondary mirror directly. (The secondary mirror is also the stop of the Offner imaging spectrometer.)

The length between the primary mirror and object point is l_s, and u_1 and u_2 are different aperture angles. The semi-diameter of the secondary mirror, h_1, is described as

$$h_1 = \frac{l_s \tan(u_1)}{4}. \tag{1}$$

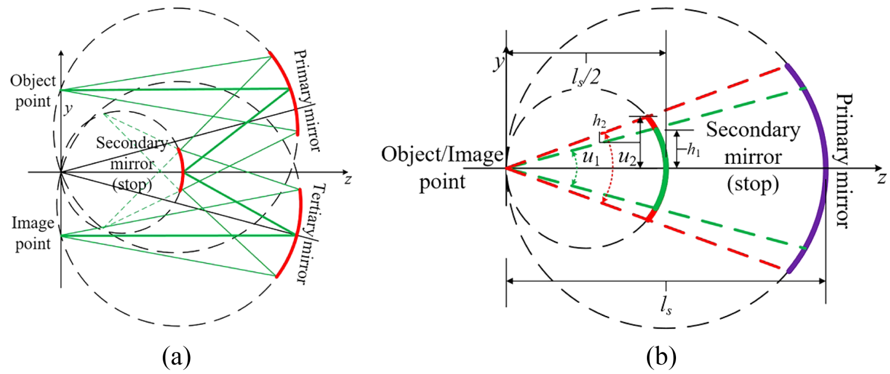

Fig. 2. Relationship between the NA and stop diameter in the Offner imaging spectrometer: (a) off-axis; (b) on-axis.

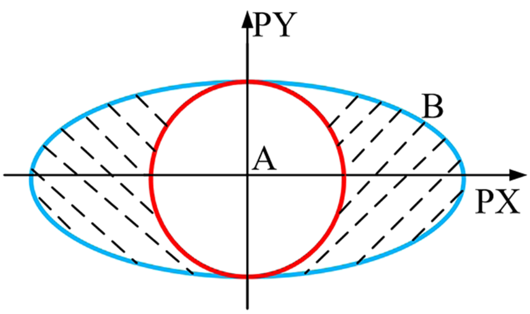

Fig. 3. Schematic diagram of the anamorphic stop.

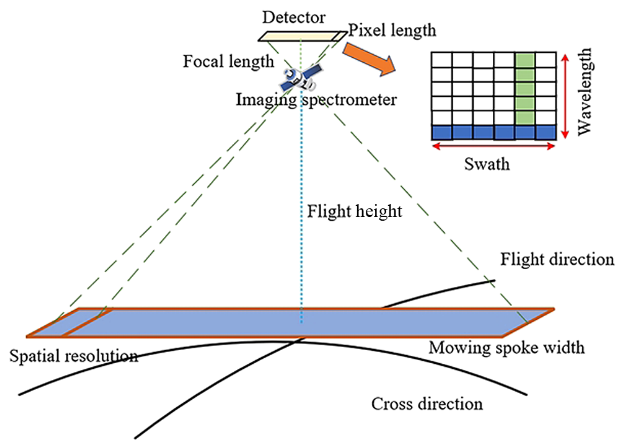

Fig. 4. Spatial resolution of the Offner imaging spectrometer.

When the structure length is constant, the semi-diameter of the secondary mirror can replace the NA. Therefore, it is feasible to characterize the NA of the Offner imaging spectrometer by discussing the secondary mirror size. And it is also reasonable to represent the light-gathering capacity of the Offner imaging spectrometer by the area of the stop.

Circular aperture stops are commonly used in Offner imaging spectrometers. In a limited system in the tangential direction, increasing the NA in the tangential direction results in light obscuration. To solve this problem, the off-axis needs to be increased, but this, in turn, produces a large aberration. Using an anamorphic stop is an effective solution. Increasing the NA along the sagittal direction can also achieve the objective of increasing the NA of the system to improve the signal-to-noise ratio (SNR) even when the NA in the tangential direction remains unchanged. The red curve in Fig. 3 represents a circular stop, the blue curve is an anamorphic stop, and the shaded part is the increased stop area.

However, in an optical system, the resolution is affected by the NA parameter. Hence, we must investigate the effect of the anamorphic stop on the spatial and spectral resolution of the Offner imaging spectrometer.

In the classical optical aberration theory, the calculation method of the resolution of the optical system is determined by the characteristics of the system. The imaging spot radius of the diffraction-limited optical system is smaller than the Airy disk, such as a microscope, telescope, and lithography object lens, and the resolution is defined by the Airy disk. Optical systems with large NA have higher resolution. Both the capacity of the light gathering and resolution will be affected when adjusting the NA of the system.

The Offner imaging spectrometer is a non-diffraction-limited system, the imaging spot radius is larger than the Airy disk, and the resolution is not constrained by the Airy disk. The remote sensing detection mode of the Offner imaging spectrometer is shown in Fig. 4.

The spatial resolution of the Offner imaging spectrometer d is defined by the flight height H, focal length f', and pixel size a, which is written as

$$d = \frac{a}{f'} H. \tag{2}$$

In addition, the average spectral resolution $d\lambda$ of the instrument can be determined by the spectral range $\Delta\lambda$, the size of the dispersion l_λ, and the pixel size.

As shown in Fig. 5, the spectral range can be represented by the starting wavelength λ_1 and ending wavelength λ_n, which is written as

$$\Delta\lambda = \lambda_1 - \lambda_n. \tag{3}$$

And the spectral resolution is

$$d\lambda = \frac{\Delta\lambda}{l_\lambda} a. \tag{4}$$

According to Eqs. (2) and (4), in a non-diffraction-limited remote sensing Offner spectrometer, the spatial and spectral resolution of the instrument is not affected by the anamorphic

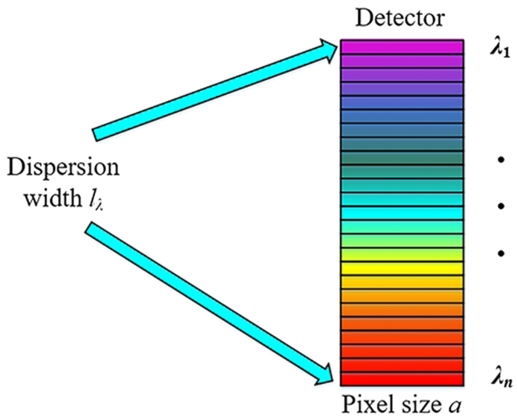

Fig. 5. Spectral resolution of the Offner imaging spectrometer.

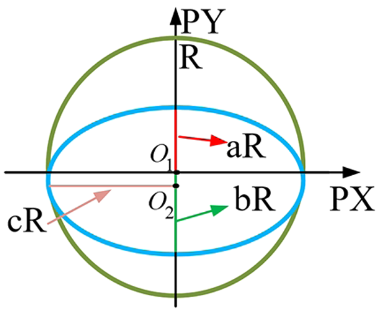

Fig. 6. Schematic diagram of the decenter anamorphic stop.

stop. Instead, in a diffraction-limited optical system, an anamorphic stop affects the resolution of the instrument, which varies with the value of the tangential and sagittal aperture.

The symmetry of the Offner structure is broken by the dispersive element. We postulate that the system parameters at the center of the anamorphic stop contribute to a certain amount of decentering. Figure 6 shows a decenter anamorphic stop closely attached to a circular stop with the radius R. The major axis represents the sagittal direction of the decenter anamorphic stop and has the length of cR, where c is a ratio coefficient with a value less than 1. The short axis represents the tangential direction, and the two tangential semiaxes that are asymmetrical relative to the center of the circular stop have the lengths of aR and bR, where a and b are coefficients.

The ratio of the area of the decenter anamorphic stop to that of the circular stop, S, is

$$S = c\left(\frac{a+b}{2}\right). \tag{5}$$

At the same time, S is also the ratio of the square f-numbers of the two stops. There are multiple sets of coefficients that meet the requirements of the design and effective f-numbers of the decenter anamorphic stop. (Obviously, not all coefficient combinations can meet these requirements.) A further choice for the best combination needs to be made. In an Offner imaging spectrometer, the distance between the edge of the tangential stop and the margin aperture beams is essentially constrained by aberration [12]. Hence, this distance can be used as the basis for choosing the best combination.

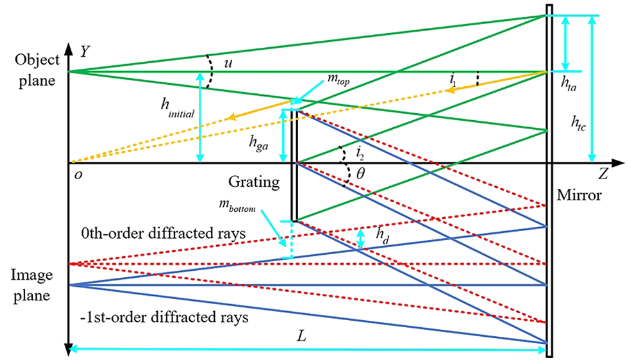

Fig. 7. Schematic diagram of the paraxial optical path of the Offner imaging spectrometer.

As shown in Fig. 7, we assume that the system is in the paraxial zone. A plane is used to simplify the system and approximate the actual optical surface. The green rays represent the reflected rays, the red rays are the zeroth-order diffracted rays from the grating, and the blue rays are the -1^{st}-order diffracted rays. We denote the aperture angle of the system as u. The object and image points are on the same plane. The origin of the system coordinates is set at the intersection of the plane and the optical axis. The distance between the mirror and the origin of the coordinates is L. The distance between the grating and the coordinate origin is $L/2$.

The projection height h_{tc} of the margin aperture ray and chief ray on the mirror is given by

$$h_{tc} = L \cdot \tan\left(\frac{u}{2}\right). \tag{6}$$

The half-width h_{ga} of the grating is given by

$$h_{ga} = \frac{L}{2} \cdot \tan\left(\frac{u}{2}\right). \tag{7}$$

The distance h_{initial} of the object point decentering from the optical axis is written as

$$h_{\text{initial}} = \frac{h_{tc}}{2} + h_{ga}. \tag{8}$$

The angle of incidence i_1 of the chief ray on the mirror is

$$i_1 = \arctan\left(\frac{h_{\text{initial}}}{L}\right). \tag{9}$$

The angle of incidence i_2 of the chief ray on the grating is

$$i_2 = 2i_1. \tag{10}$$

The diffraction angle θ of the chief ray of the grating is

$$\theta = \arcsin\left(\frac{m\lambda}{d} - \sin(i_2)\right). \tag{11}$$

The vertical distance h_d between the grating -1^{st}-order diffracted chief ray and the zeroth-order diffracted chief ray is expressed as

$$h_d = \frac{3L}{2} \cdot \left(\frac{\cos(i_2) - \cos(\theta)}{\cos(\theta) \cdot \cos(i_2)}\right) \cdot \frac{1}{\cos(u)}. \tag{12}$$

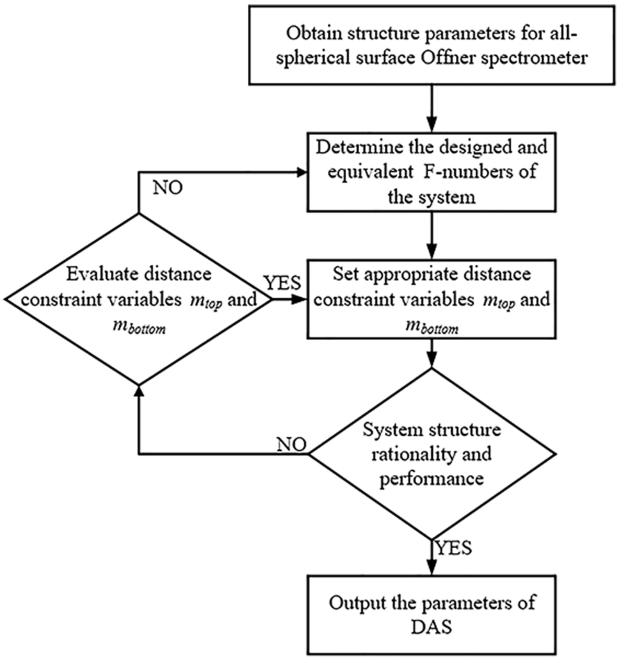

Fig. 8. Flow chart of the decenter anamorphic stop parameter calculation process.

Using Eqs. (6)–(12), the distance m_{top} and m_{bottom} between the margin aperture rays and the edge of the grating in the divergent and convergent light paths of the Offner spectrometer can be expressed as follows:

$$m_{\text{top}} = (1-b)\cdot\frac{L}{2}\cdot\tan\left(\frac{u}{2}\right) + (1-a)\cdot h_{ga},$$

$$m_{\text{bottom}} = (1-a)\cdot\frac{L}{2}\cdot\tan\left(\frac{u}{2}\right) + (1-b)\cdot h_{ga} + h_d. \quad \textbf{(13)}$$

Based on the above analysis, Eq. (13) is used as the basis for judging the decenter anamorphic stop parameters. A flow chart of the process for calculating the decenter anamorphic stop parameters is shown in Fig. 8.

3. DESIGN EXAMPLE OF AN IMAGING SPECTROMETER WITH A FREEFORM SURFACE

In our published paper [12], we designed a wide-field compact imaging spectrometer with an f-number of 3 utilizing a freeform surface. The light-gathering capacity of the spectrometer will be increased by more than 40% if the f-number of the spectrometer is increased to 2.5. This will reduce the integration time of the detector and improve the detection capability and working efficiency of the instrument.

The parameters for the decenter anamorphic stop were obtained using the design method in Section 2.A and listed in Table 1. The design specifications for the compact spectrometer with a wide FoV and large NA considered in this paper are listed in Table 2. According to Table 1 and [13], the schematic diagram of the sagittal and tangential beam aperture distribution as shown in Fig. 9 is obtained. The parameters and Fig. 9 show that it is extremely difficult to increase the beam aperture angle in the tangential direction in an Offner spectrometer under strict

Table 1. Specifications of the Decenter Anamorphic Stop

Parameters	Value	Units
Designed f-number	2.2	—
Effective f-number	2.5	—
Tangential NA	0.169	—
Sagittal NA	0.225	—
Tangential decenter	−0.038793	mm

Table 2. Specifications of the Imaging Spectrometer

Parameters	Value	Units
Spectral range	400–1000	nm
Effective NA	0.2	—
Slit length	22.5	mm
Detector pixel size	11 × 11	μm
Spectral resolution	≤2.7	nm
Spectrometer length	≤85	mm
Spectral channel	≥222	—

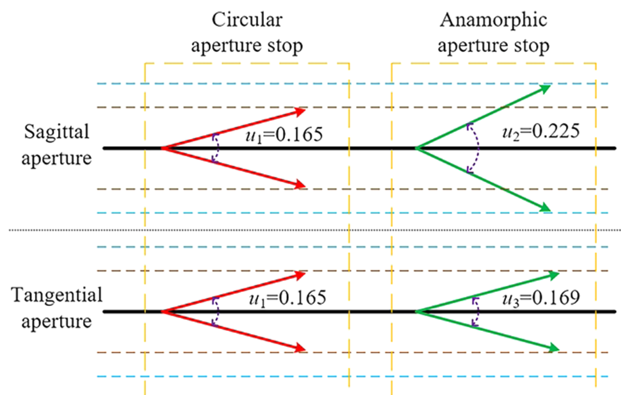

Fig. 9. Schematic diagram of the sagittal and tangential beam aperture distribution.

system size constraints. However, the beam aperture angle in the sagittal direction can be further increased so that the aberration correction function of the freeform surface will be fully utilized in an Offner freeform surface spectrometer with the decenter anamorphic stop.

In addition, the value of the aperture angle affects the clear aperture of the optical element when the length of the Offner spectrometer is constant. As shown in Fig. 10, the length between the slit and the primary mirror is l, and u_1 and u_2 are the sagittal aperture angle of the circular aperture stop and anamorphic aperture stop, respectively. The increased area in the clear aperture of the primary mirror, Δs, is expressed as

$$\Delta s = 4l^2\left(\tan\left(\frac{u_2}{2}\right) - \tan\left(\frac{u_1}{2}\right)\right)\tan\left(\frac{u_1}{2}\right). \quad \textbf{(14)}$$

According to Eq. (14), the size of the Offner spectrometer with an anamorphic stop is broadened in the sagittal direction, and there is a slight increase in volume.

However, the increment of the sagittal aperture angle is limited. In the paper, we investigate the image RMS value of the initial structure of the Offner imaging spectrometer with a

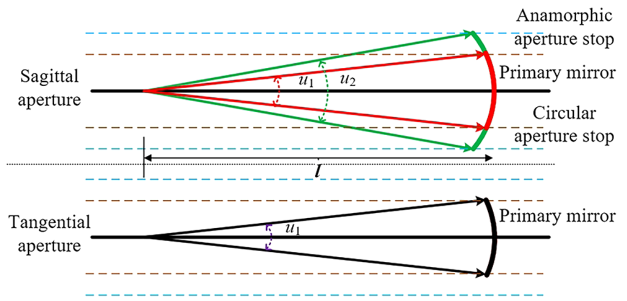

Fig. 10. Schematic diagram of the clear aperture of the optical element in the Offner imaging spectrometer with an anamorphic stop.

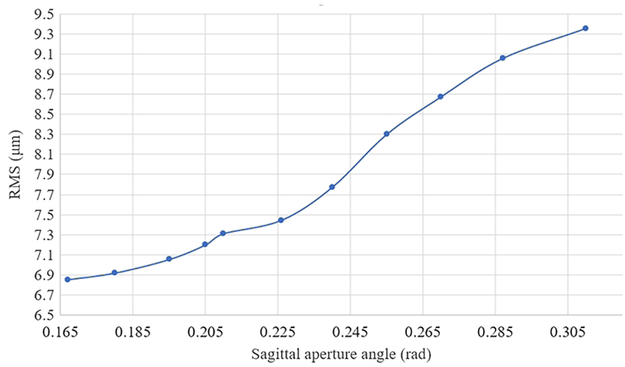

Fig. 11. Analysis curve of the relationship between the sagittal aperture angle and the RMS value of the initial structure of the Offner imaging spectrometer.

sagittal aperture angle in the range of 0.165 to 0.305, when the other parameters are constant. The analysis curve is shown as Fig. 11, when the sagittal aperture angle is between 0.165 and 0.225, the RMS value of the Offner imaging spectrometer varies less. And when the sagittal aperture angle is between 0.225 and 0.305, the RMS value of the Offner imaging spectrometer varies greatly. In the design, a larger effective NA can be obtained by using a larger sagittal aperture angle. But the RMS value of the Offner imaging spectrometer is larger at this time, so it is difficult to obtain the design result with good image quality, even using a freeform surface. To balance the optimization potential of the initial structure and the value of the effective NA, the sagittal aperture angle between 0.205 and 0.225 is optimal, which is consistent with the calculation results in Table 1. This means that 0.2 effective NA is the design limit under the specifications in Table 2. Therefore, this increase in volume caused by designing an Offner imaging spectrometer with a decenter anamorphic stop is unavoidable but acceptable.

Using the decenter anamorphic stop parameters, we obtained design results that meet the requirements after a few optimizations. A schematic of the imaging spectrometer is shown in Fig. 12. The rays are reflected by the primary mirror to the convex grating, which is located at the secondary mirror. The direction of the convex grating grooves is parallel to the XoZ plane and perpendicular to the diffraction direction. The rays are subsequently dispersed into rays of different wavelengths, which are focused by the freeform tertiary mirror, and then

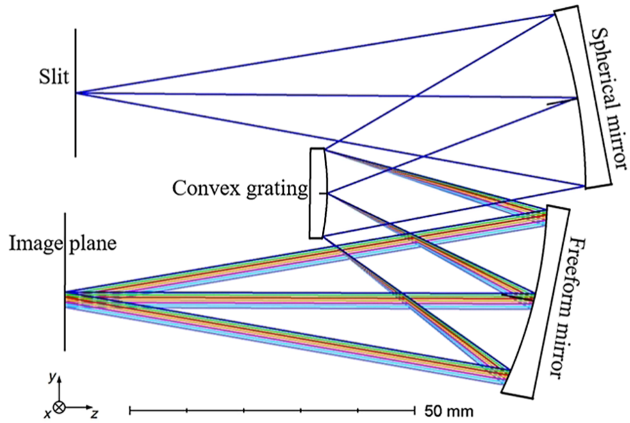

Fig. 12. Structure of the imaging spectrometer with freeform optics.

Table 3. Basic Parameters of the Spectrometer

Surface	Surface Type	Radius (mm)	Thickness (mm)	Material
1	object plane	—	85	—
2	spherical	−84.97	−44.21	mirror
4	convex grating	−40.35	37.96	mirror
5	*xy* polynomial	−78.56	−78.74	mirror
10	image plane	—	—	—

Table 4. Freeform Surface Coefficients of Tertiary Mirror

Term	Coefficient a_i	Term	Coefficient a_i	Term	Coefficient a_i
x^2y^0	$-7.6514e^{-6}$	x^0y^4	$1.0234e^{-9}$	x^2y^4	$-1.0828e^{-11}$
x^0y^2	$1.2574e^{-6}$	x^4y^1	$1.2092e^{-10}$	x^0y^6	$-3.6402e^{-11}$
x^2y^1	$-1.2506e^{-7}$	x^2y^3	$-1.3636e^{-10}$	x^6y^1	$1.5621e^{-12}$
x^0y^3	$1.7692e^{-8}$	x^0y^5	$-1.2639e^{-10}$	x^4y^3	$2.7775e^{-12}$
x^4y^0	$2.0707e^{-9}$	x^6y^0	$-1.1414e^{-11}$	x^2y^5	$-4.1473e^{-13}$
x^2y^2	$-2.2993e^{-8}$	x^4y^2	$3.6846e^{-11}$	x^0y^7	$-1.0064e^{-12}$

received by the detector at the image plane. The basic parameters of the spectrometer are listed in Table 3, and the coefficients of the freeform surface are in Table 4.

The overall size of the system in [13] was 85 × 64 × 56 mm^3. The overall size of the spectrometer designed in this study is 85 × 66 × 65 mm^3. Although the length of the system is unchanged, the volume is increased by approximately 19%. However, the light-gathering capacity of the system is increased by more than 40%. Offner freeform optics spectrometers utilizing the decenter anamorphic stop show excellent potential for compact designs with wide FoV and large NA.

In addition, as shown in Fig. 13, the increased area of the freeform mirror is covered by the beam of the margin field of the imaging spectrometer. The aberration correction of the beam of the margin field is important, and it is related to the success or failure of the design. Based on the aberration correction principle of the *xy* polynomial freeform surface, the surface edge shape of the optical element is more obviously affected by the higher-order polynomials. Compared with [12], in the

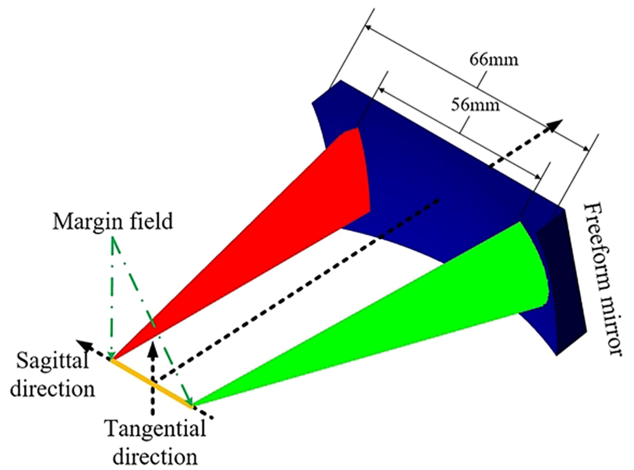

Fig. 13. Schematic diagram of the various area of the freeform mirror.

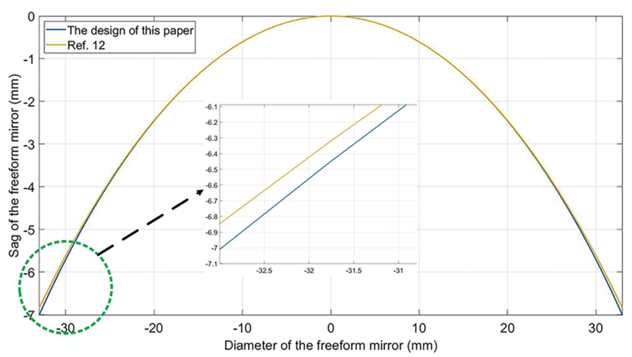

Fig. 14. Variation curve of the freeform mirror sag.

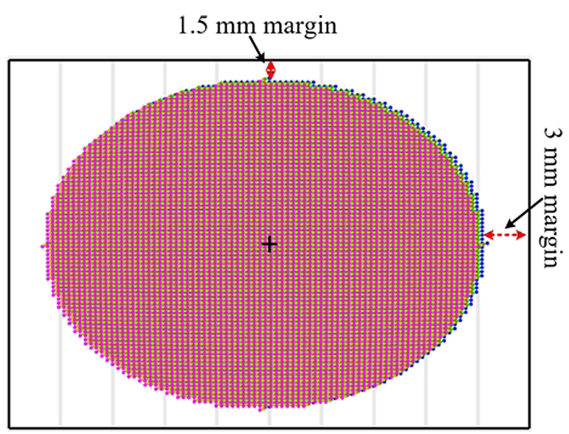

Fig. 15. Footprint diagram of the convex grating.

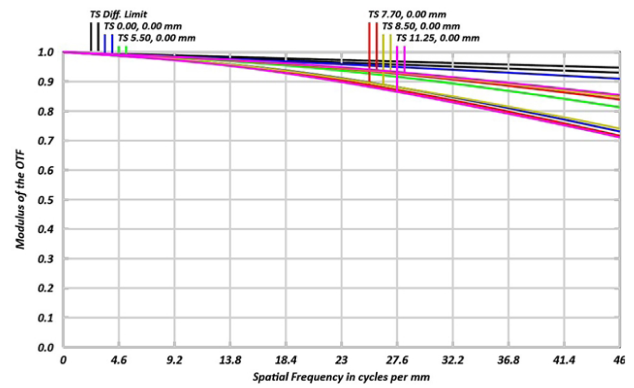

(a)

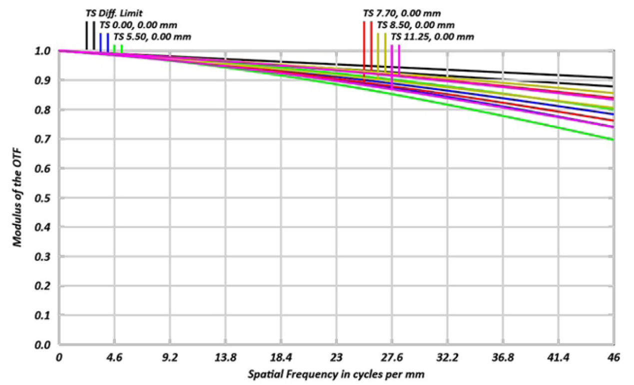

(b)

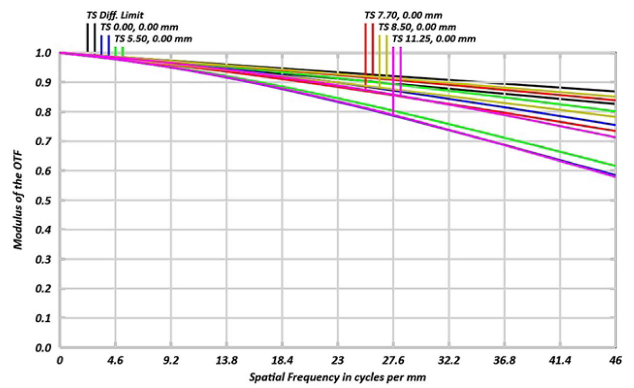

(c)

Fig. 16. MTFs of spectrometer at (a) 400 nm, (b) 700 nm, and (c) 1000 nm.

paper, the high-order polynomials of the freeform surface create a larger sag deviation in the mirror edge as shown in Fig. 14. Hence, the freeform surface sag deviation of the Offner imaging spectrometer with a decenter anamorphic stop is higher. Besides, at the freeform mirror edge, the variation rate of the surface gradient of the Offner imaging spectrometer with a decenter anamorphic stop is larger. Therefore, the freeform mirror of the Offner imaging spectrometer with a decenter anamorphic stop is more difficult to fabricate and measure. In the design, we need to pay attention to the manufacturability of the freeform mirror. Depending on the available fabrication and metrology technologies, we balance the performance of the instrument with the fabrication of the freeform surface to obtain the best design result.

A footprint diagram of the grating is shown in Fig. 15. Because of the decenter anamorphic stop, the determined shape of the grating is rectangular, which is generally considered to be easier to test and align. We reserve 1.5 mm and 3 mm at the tangential and sagittal effective aperture peripheries of the convex grating, respectively, to ensure that the marginal surface accuracy of the grating is not affected by the alignment.

The modulation transfer functions (MTFs) for different wavelengths are shown in Figs. 16(a)–16(c). All the MTFs at

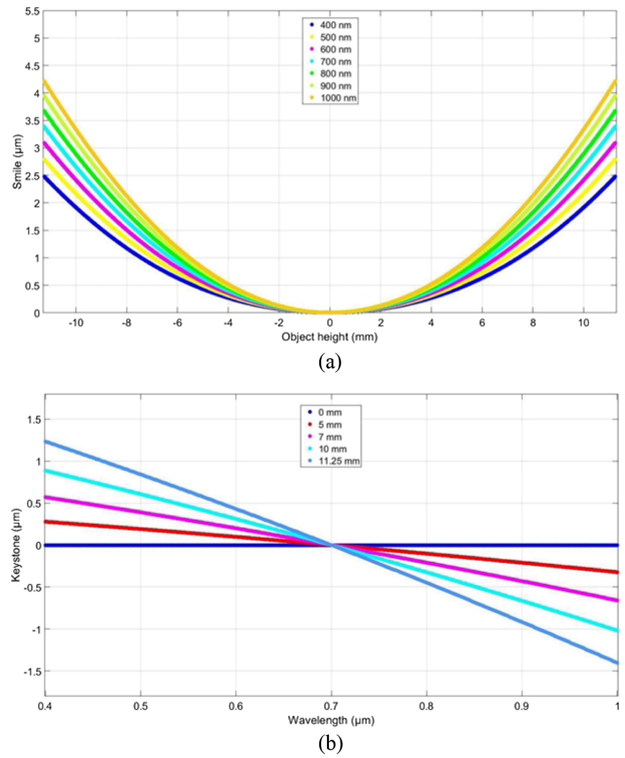

Fig. 17. (a) Spectral smile at different wavelengths and (b) keystone at different FoVs.

the Nyquist frequency exceed 0.58. This indicates that the energy utilization of the spectrometer is high, which is helpful for improving the SNR.

Spectral smiles and keystones are two types of spectrometer distortions that occur at different FoVs and wavelengths. We reduced the distortion by optimizing the curvature, decenter, and tilt of the optical elements. The spectral smile and keystone are shown in Figs. 17(a) and 17(b), respectively. At the wavelength of 1000 nm, the maximum spectral smile is less than 0.43 pixels. At the FoV of 11.25 mm, the maximum keystone is less than 0.12 pixels. The spectral resolution of the spectrometer is shown in Fig. 18. The average spectral resolution is 2.496 nm. These results show that the requirements of the spectrometer are satisfied and are consistent with [12].

The image quality of the different wavelengths is different in the imaging spectrometer. Thus, it is necessary to execute an investigation of the tolerance for different wavelengths. In the section, the criterion of the MTF degradation is accepted

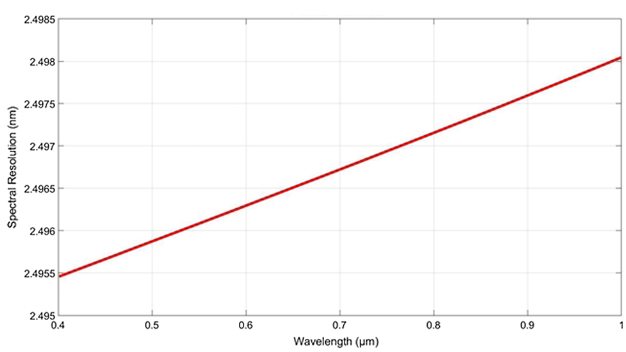

Fig. 18. Spectral resolution at different wavelengths.

Table 5. Tolerance Analysis at 400 nm

Tolerance Items	Element	Given Value	Change of MTF
Element x-decenter (mm)	Freeform mirror	−0.02	0.039
Element y-tilt (degree)	Freeform mirror	0.01	0.037
Element x-decenter (mm)	Spherical mirror	0.02	0.034
Element y-tilt (degree)	Spherical mirror	−0.01	0.03
Element y-decenter (mm)	Freeform mirror	0.02	0.027
Conic	Freeform mirror	0.003	0.025
Element x-tilt (degree)	Spherical mirror	0.01	0.022
Element y-decenter (mm)	Spherical mirror	−0.02	0.019

Table 6. Tolerance Analysis at 1000 nm

Tolerance Items	Element	Given Value	Change of MTF
Element y-decenter (mm)	Freeform mirror	−0.02	0.031
Element x-tilt (degree)	Freeform mirror	−0.01	0.028
Element y-decenter (mm)	Spherical mirror	0.02	0.025
Element x-tilt (degree)	Spherical mirror	0.01	0.023
Element x-decenter (mm)	Freeform mirror	0.02	0.019
Element y-tilt (degree)	Freeform mirror	−0.01	0.016
Radius (mm)	Freeform mirror	−0.003	0.015
Element x-decenter (mm)	Spherical mirror	−0.02	0.013

as 0.2. Based on sensitivity and Monte Carlo tolerance analysis methods, we have listed eight factors that have a significant impact on the tolerance at 400 nm and 1000 nm in Tables 5 and 6, respectively. The RMS of the primary mirror surface irregularity is better than $\lambda/40$ ($\lambda = 632.8$ nm), and the RMSs of the convex grating and freeform tertiary mirror surface irregularity are better than $\lambda/30$. The MTF simulation results are shown in Figs. 19(a) and 19(b), which are obtained after 500 Monte Carlo simulation runs. The result for 400 nm shows a 90% probability that the MTF changed by only 0.12, and the analysis of 1000 nm shows a 90% probability that the MTF changed by only 0.09. All the given tolerances meet the metrology, fabrication, and alignment capabilities of the current freeform optical systems. Tolerance analysis results show that the designed Offner imaging spectrometer with a freeform mirror can be successfully fabricated.

4. FABRICATION OF THE FREEFORM SURFACE

In this work, we fabricated and measured the freeform mirror of Section 3. The mechanical diameter of the freeform mirror is 66 mm × 40 mm. The residual surface sag after removing the best-fit sphere is shown in Fig. 20. The yellow curve in the green box area is the sag curve within the clear aperture of the freeform mirror in the tangential direction, and the blue curve is the sag curve of the freeform mirror in the sagittal direction. The maximum surface departure from the best-fit sphere of the freeform mirror is 39 μm PV in the sagittal direction and 17 μm PV in the tangential direction. The freeform surface was produced on a Precitech Nanoform 700 machine, which provides ultra-high machining accuracy. The diamond tool radius is 0.512 mm, with a rake angle of 0 deg. The machine is run with a speed of 1200 rpm, a feed rate of 2.2 mm/min, and a depth cut of 2 μm. Super-clean aluminum 6061 has less weight, good acceptance of

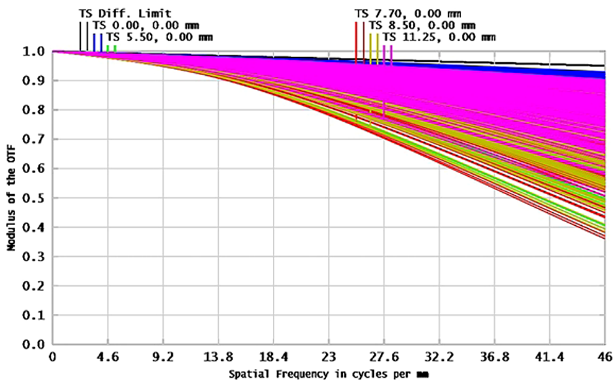

(a)

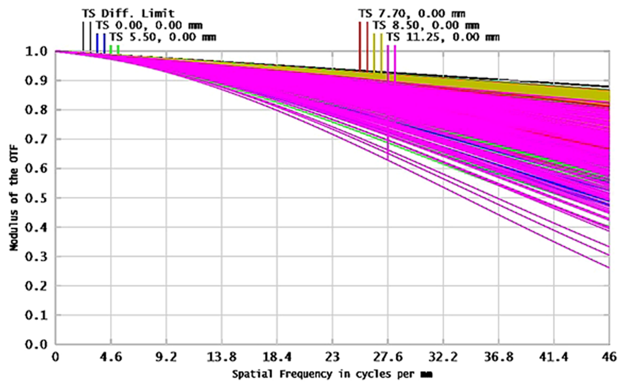

(b)

Fig. 19. Tolerance simulation results of Monte Carlo simulation: (a) 400 nm and (b) 1000 nm.

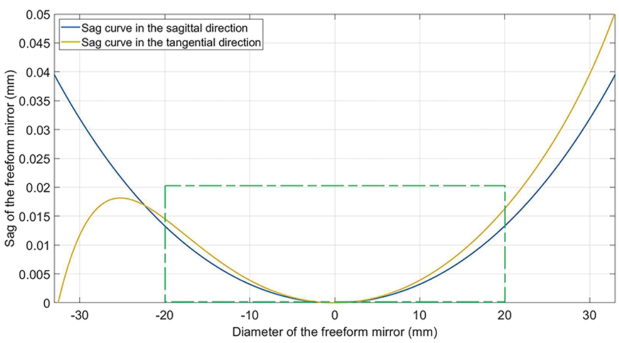

Fig. 20. Residual surface sag is after removing the best-fit sphere.

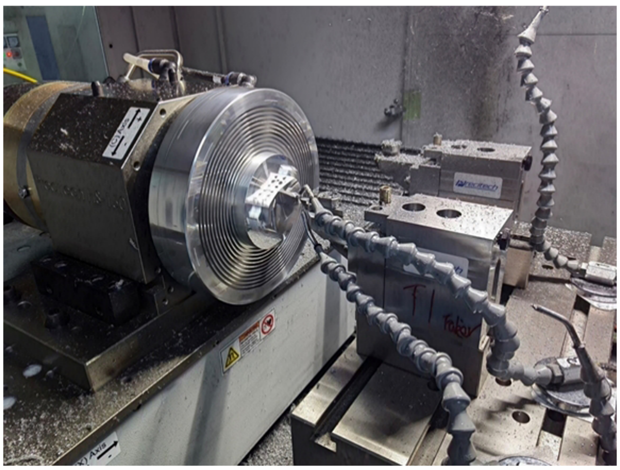

Fig. 21. Freeform mirror machined with single point diamond turning technology.

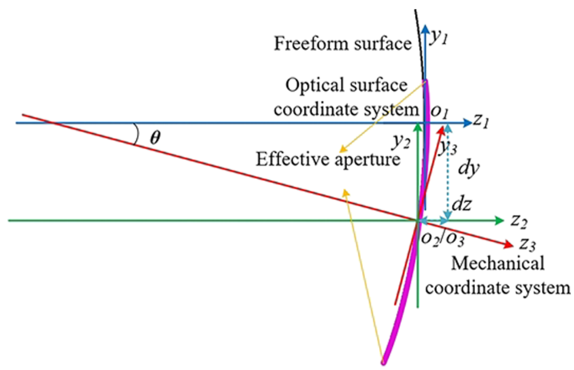

Fig. 22. Conversion relationship between the optical coordinate and mechanical coordinate.

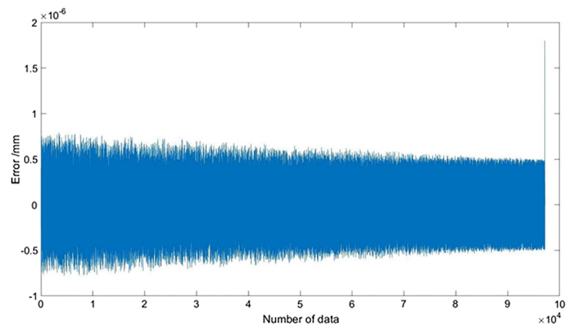

Fig. 23. Error curve of the machining data points.

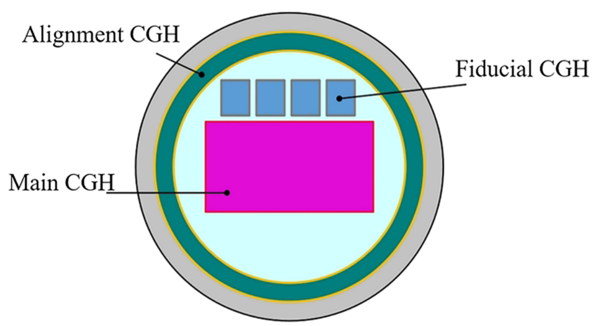

Fig. 24. Layout of CGH function.

applied coatings, relatively high strength, and high resistance to corrosion, and it is used as a material for the freeform surface. As shown in Fig. 21, the raw material is milled and rough machined to shape, and then it is finished on the machine.

Before finishing, we need to complete the work of tool alignment, machining data generation, etc. As shown in Fig. 22, there is decenter between the effective aperture center of the freeform surface and the optical aperture center. The optical coordinate system $y_1 o_1 z_1$ needs to be transformed by translation and

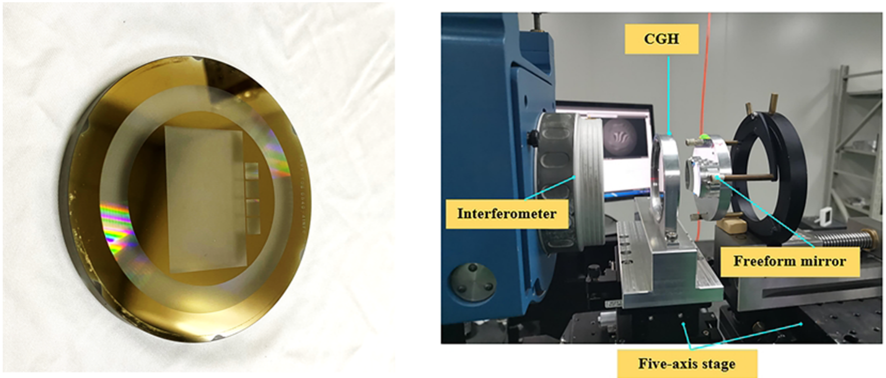

(a) (b)

Fig. 25. (a) Designed CGH; (b) metrology of the freeform mirror.

rotation to obtain the mechanical coordinate system $y_3o_3z_3$. According to the freeform surface equation, the machine software generates a large number of machining data points. However, there are some biases in these data points. We need to check to ensure that the generated data points are accurate. In the software, about 100,000 machining data points were generated. By calculating the error of each data point, it is concluded that about 15 data points have a maximum error of about 2 nm, and the remaining data points have a maximum error of about 0.65 nm, with an average value of $-2.986e^{-4}$ nm. As shown in Fig. 23, the error curves show that the generated freeform data points have a small conversion error and can be used for actual machining.

Currently, the most challenging component in the construction of a freeform imaging system is the metrology of the freeform surfaces [18]. In this paper, a CGH-based interferometric null test method is used to measure the freeform surface. Compared with other metrology methods, CGH is more accurate and reliable. The designed CGH consists of three main functional regions, including the main region, the alignment region, and the fiducial region, as shown in Fig. 24. In particular, the main CGH is used to create a wavefront that matches the freeform surface and can provide better than $1/30\lambda$ of the metrology accuracy. As shown in Fig. 25(a), the CGH was prepared using quartz material, and the diameter is 80 mm. Both the freeform surface and CGH are fixed on the five-axis platform by the fixture, as shown in Fig. 25(b). By the surface test optical path built by the ZYGO interferometer, we can obtain accurate surface metrology results.

Aluminum has the advantage that tool wear in diamond machining is nearly non-existent. However, its mechanical properties lead to some undesirable effects such as the formation of large burrs at the tool–material interaction points [15]. In addition, single point diamond turning (SPDT) often creates mid-spatial frequency errors on the surface of optical components. As shown in Fig. 26, the RMS of the finished freeform surface is about $1/10\lambda$, and PV is about $1/2\lambda$. The freeform surface has obvious periodic-type mid-spatial frequency errors. Then the freeform surface is polished by manual means. During polishing, the freeform surface is rechecked several times until the required machining results are obtained. After that, films with 99.97% reflectivity are plated on the freeform surface.

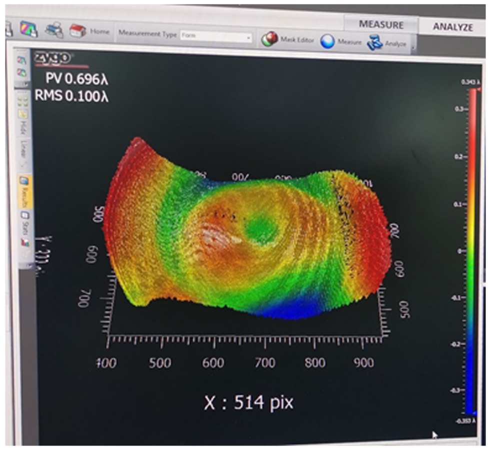

Fig. 26. Measurement result of the freeform mirror after turning.

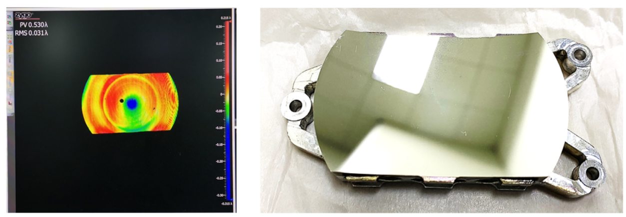

(a) (b)

Fig. 27. (a) Final metrology result of the freeform mirror; (b) finished freeform mirror.

The final metrology result of the freeform surface is shown in Fig. 27(a), the surface irregularity of the freeform surface is better than $1/30\lambda$, and the finished freeform surface is shown in Fig. 27(b).

5. CONCLUSION AND OUTLOOK

In this paper, we present a method for designing a freeform spectrometer with a decenter anamorphic stop based on insights from the limited system in the tangential direction concept. A compact imaging spectrometer with a wide FoV and a large NA was designed using the method. The light-gathering capacity was improved by more than 40%. At the same time, we investigate the spatial and spectral resolution of the freeform Offner imaging spectrometer with the decenter anamorphic stop. The result is that the spatial and spectral resolution of the instrument is not influenced by using decenter anamorphic stop. We also fabricated and measured the freeform mirror. The process of the fabrication and the result of the metrology are introduced, respectively. The result shows that the surface irregularity of the freeform tertiary mirror is better than $1/30\lambda$.

We will next explore further high-efficiency alignment methods for the freeform surface spectrometers, improved preparation and detection methods, and faster and more simplified processing routes for such spectrometers. We will also explore cost reduction, which is essential for furthering the market applications of imaging spectrometers with freeform optics. In conclusion, the design method for an Offner imaging spectrometer with a decenter anamorphic stop in this paper exploits the aberration correction abilities of the freeform surface fully and is greatly significant for the design of compact wide-FOV and large-NA Offner imaging spectrometers that utilize freeform surfaces.

Funding. National Key Research and Development Program of China (2021YFB3901000); Scientific Instrument Developing Project of the Chinese Academy of Sciences (YJKYYQ20190047).

Disclosures. The authors declare that they have no conflicts of interest related to this paper.

Data availability. The data that support the findings of this study are available from the authors upon reasonable request.

REFERENCES

1. J. M. Rodgers and K. P. Thompson, "Benefits of freeform mirror surfaces in optical design," in *Proceeding of the American Society of Precision Engineering 2004 Winter Topical Meeting on Freeform Optics* (2004), pp. 73–78.
2. F. Fang, X. Zhang, A. Weckenmann, G. Zhang, and C. Evans, "Manufacturing and measurement of freeform optics," CIRP Ann. **62**, 823–846 (2013).
3. H. Ries and J. Muschaweck, "Tailored freeform optical surfaces," J. Opt. Soc. Am. A **19**, 590–595 (2002).
4. J. Chaves, *Introduction to Nonimaging Optics* (CRC press, 2017).
5. R. Geyl, E. Ruch, R. Bourgois, R. Mercier-Ythier, H. Leplan, and F. Riguet, "Freeform optics design, fabrication, testing technologies for space applications," Proc. SPIE **11180**, 111800P (2019).
6. E. M. Schiesser, A. Bauer, and J. P. Rolland, "Effect of freeform surfaces on the volume and performance of unobscured three mirror imagers in comparison with off-axis rotationally symmetric polynomials," Opt. Express **27**, 21750–21765 (2019).
7. T. Peschel, C. Damm, M. Beier, A. Gebhardt, S. Risse, I. Walter, I. Sebastian, and D. Krutz, "Design of an imaging spectrometer for earth observation using freeform mirrors," Proc. SPIE **10562**, 1056237 (2016).
8. J. Reimers, A. Bauer, K. P. Thompson, and J. P. Rolland, "Freeform spectrometer enabling increased compactness," Light Sci. Appl. **6**, e17026 (2017).
9. T. Yang, D. Cheng, and Y. Wang, "Freeform imaging spectrometer using a point-by-point design method," Appl. Opt. **57**, 4718–4727 (2018).
10. L. Feng, J. Zhou, L. Wei, X. He, Y. Li, J. Jing, and B. Xiangli, "Design of a compact wide-spectrum double-channel prism imaging spectrometer with freeform surface," Appl. Opt. **57**, 9512–9522 (2018).
11. D. R. Shafer and L. Gilles, "Freeform aspheric version of the Offner1.0X relay," in *Design and Fabrication Congress* (2019), paper JT3B.
12. J. Zhang, Y. Zheng, C. Lin, Z. Ji, and H. Wu, "Analysis method of the Offner hyperspectral imaging spectrometer based on vector aberration theory," Appl. Opt. **60**, 264–275 (2021).
13. M. P. Chrisp, "Convex diffraction grating imaging spectrometer," U. S. patent5,880,834A (March 9, 1999).
14. A. Offner, "New concepts in projection mask aligners," Opt. Eng. **14**, 130–132 (1975).
15. D. Xu, J. D. Owen, J. C. Papa, J. Reimers, T. J. Suleski, J. R. Troutman, M. A. Davies, K. P. Thompson, and J. P. Rolland, "Design, fabrication, and testing of convex reflective diffractive grating," Opt. Express **25**, 15252–15267 (2017).
16. K. Fuerschbach, J. P. Rolland, and K. P. Thompson, "Theory of aberration fields for general optical systems with freeform surfaces," Opt. Express **22**, 26585–26606 (2014).
17. E. Miller, G. Klein, D. Juergens, K. Mehaffey, J. Oseas, R. Garcia, A. Giandomenico, B. Irigoyen, R. Hickok, D. Rosing, H. Sobel, and C. Bruce, "The visual and infrared mapping spectrometer for Cassini," Proc. SPIE **2803**, 206–220 (1996).
18. Y. J. Xie, X. L. Mao, J. P. Li, F. B. Wang, P. Wang, R. Gao, X. Li, S. J. Ren, Z. C. Xu, and R. G. Dong, "Optical design and fabrication of an all-aluminum unobscured two-mirror freeform imaging telescope," Appl. Opt. **59**, 833–840 (2020).